

TECHNICAL REPORT
DRI #2671
2 February 1976

②
REPORT

AD-A148 242

E-M RADIATION FROM CORONA DISCHARGES

20000804059

DTIC
ELECTE
DEC 5 1984
S A D

DTIC FILE COPY

**APPROVED FOR PUBLIC RELEASE:
DISTRIBUTION UNLIMITED**

UNIVERSITY OF DENVER • DENVER RESEARCH INSTITUTE

Reproduced From
Best Available Copy

84 11 28 083

TECHNICAL REPORT

E-M Radiation from Corona Discharges

Contract: N00019-74-C-0334

- Sponsored by -

Naval Air Systems Command
Washington, D. C. 20360

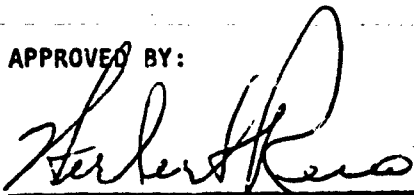
- Performed by -

Electronics Division
Denver Research Institute
University of Denver
Denver, Colorado 80210

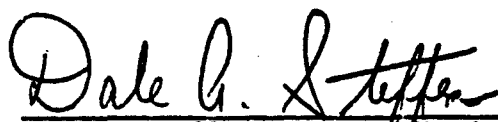
2 February 1976

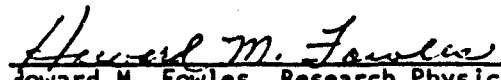
APPROVED FOR PUBLIC RELEASE:
DISTRIBUTION UNLIMITED

APPROVED BY:


Herbert Reno
Electronics Division

PREPARED BY:


Dale A. Steffen, Research Physicist
Electronics Division


Howard M. Fowles, Research Physicist
Electronics Division

CONTENTS

	<u>Page</u>
LIST OF FIGURES	iii
I. INTRODUCTION	1
II. EXPERIMENTAL WORK.	2
A. R-f energy from a corona point.	2
B. Corona from the end of a cylindrical conductor.	4
1. Description of experiments	4
2. Current distribution	4
3. Corona pulse rate and charging current	6
4. R-f radiation.	8
C. Radio noise survey.	13
1. Description of experiments	13
2. Results.	15
D. Field measurements on low flying aircraft	15
1. Description of experiments	15
2. Results.	17
III. ANALYSIS	18
A. The corona current in air	18
B. The corona current on a conducting cylinder	19
C. The radiated fields	20
IV. CONCLUDING REMARKS	30
REFERENCES	31



Division For	
NO. GRAF	<input checked="" type="checkbox"/>
NO. TAB	<input type="checkbox"/>
NO. INDEXED	<input type="checkbox"/>
NO. IDENTIFICATION	<input type="checkbox"/>
Contributor	
Availability Code	
Avail and/or Special	
A-1	

LIST OF FIGURES

<u>Figure No.</u>		<u>Page</u>
1	R-f Emission from a Corona Point in Air.	3
2	Negative Point Corona Current Pulse.	5
3	Current Distribution on a 20 foot Pipe	7
4	Corona Pulse Rate versus Pipe Potential.	9
5	Charging Current versus Pipe Potential	10
6	R-f Power Received from a 10 foot Pipe in Corona . . .	11
7	Detected I.F. Signals Received from a 20 foot Pipe in Corona	14
8	Background Noise Spectrum measured at Sea.	16
9	Calculated Current Pulse on a Cylinder	21
10	Source Geometry.	20
11	Radiated Pulse from Corona Electron Currents in Air. .	23
12	Synthesis of the Radiated Pulse Train by Convolution .	27

1

I. INTRODUCTION

Precipitation static generated on aircraft by corona discharges has long been recognized as a major problem in the design of noise-free radio communication systems. However, little attention has been given to the radiated electromagnetic fields that accompany the discharge process. This report describes work performed by the Denver Research Institute in the investigation of the electromagnetic fields radiated by conducting bodies in corona.

Corona discharges occur in the strong local electric field which builds up around the edges of an airframe as the airframe potential rises from the impact of precipitation particles or other charging mechanisms. The discharges create avalanche currents in the air and launch transient current pulses on the airframe which travel from the discharge point to the open ends of the airframe where they are reflected. The airframe thus behaves like a pulsed transmission line and radiates whenever the current pulses encounter a change in impedance due to changes in the geometrical or electrical characteristics of the airframe.

The local fields produced by the traveling current pulses couple strongly into on-board antennas and produce p-static. The radiated field components are negligible by comparison and are not usually an important source of p-static receiver noise.

The investigation of e-m radiation from corona discharges has covered a broad range of experimental and analytical work. The work has included studies of the radiation from corona currents in air and from point discharges at one end of a charged conducting cylinder, field measurements of the natural noise environment at sea, and some observations of signals associated with low flying commercial aircraft.



II. EXPERIMENTAL WORK

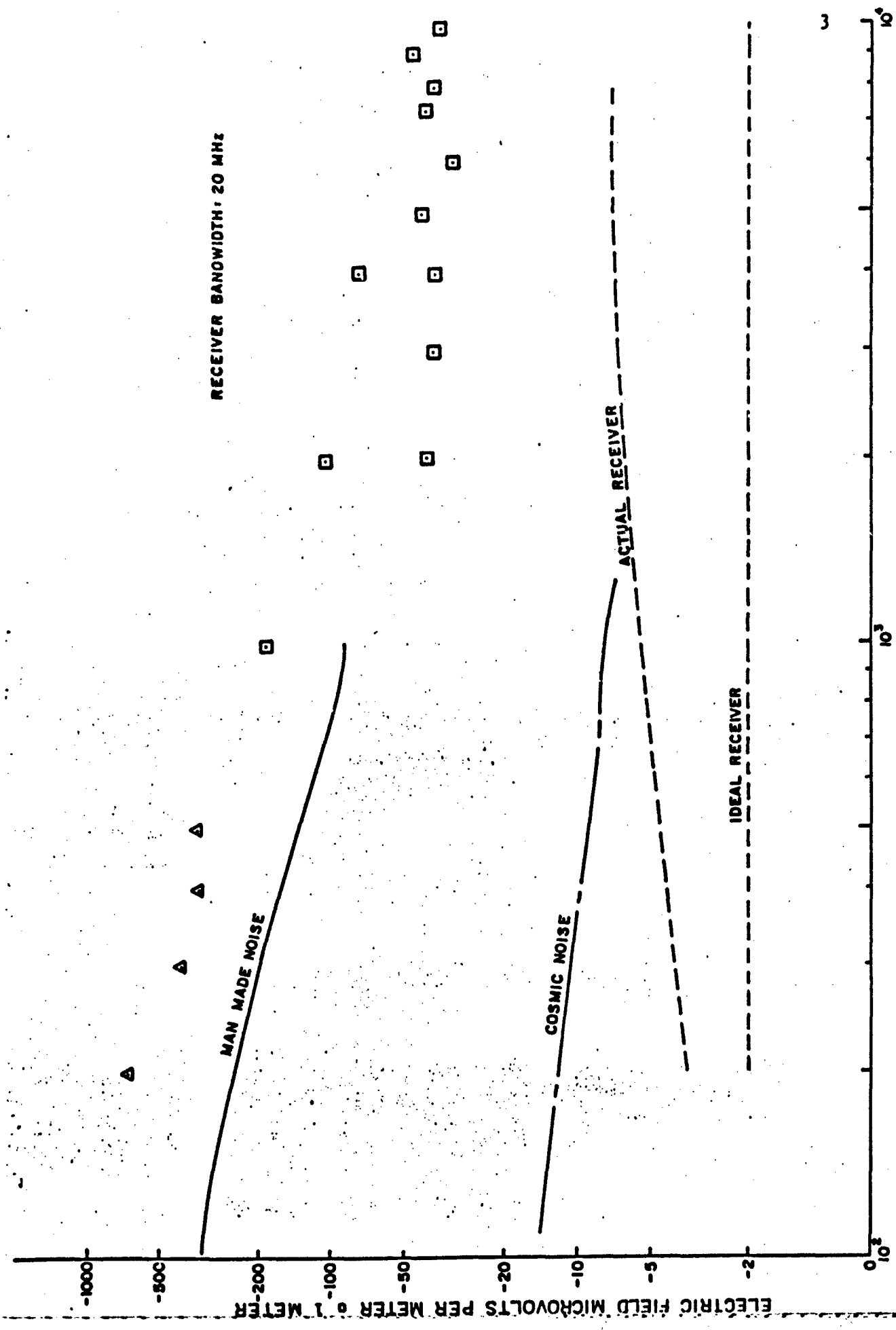
A. R-f energy from a corona point

An investigation of the power radiated in the 30 MHz to 9 GHz frequency range by corona point discharges in air was carried out at the Cherry Creek Field Site Southeast of Denver after a receiving system was assembled from available components. The system utilized an HP8555 Spectrum Analyzer as the receiver and various electric field probes and microwave horn antennas as sensors. The system sensitivity was approximately -90 dbm for a 300 kHz bandwidth, the widest bandwidth available on the HP8555 analyzer. The experiments were performed inside a shielded metal building to reduce the interference from commercial radio transmissions.

R-f energy at frequencies below 150 MHz was found to be detectable at a distance of 1 meter from the corona point with this recording system. However, no signal power could be detected at higher frequencies due to the relatively high level of internal system noise above 150 MHz.

The microwave measurements were repeated at Fort Huachuca, Arizona, using equipment with a better signal to noise ratio and a wider bandwidth which was borrowed from ASATEC. This receiving system utilized a Microtel receiver with a 20 MHz bandwidth for the 1 to 10 GHz frequency range and a Watkins-Johnson receiver with a 3 MHz bandwidth to cover frequencies below 1 GHz. Various TWT preamplifiers were used to increase the system gain.

R-f energy from the corona point was found to be detectable with this receiving system over the entire frequency range studied. The results are shown in Figure 1 as a function of frequency with the measurements below 1 GHz scaled as $\sqrt{20/3}$ to account for the different bandwidths used. Actual measurements at different bandwidths indicated that the signal amplitude increased with bandwidth somewhat more than proportional to the square root of bandwidth.



5
 FIGURE 5 R-F EMISSION FROM A CORONA POINT IN AIR

The corona current was monitored during the experiments by measuring the voltage pulse across a 50 ohm high frequency disk resistor. A typical current pulse recorded with a Tektronix R7912 Transient Digitizer with a rise time of approximately 1 nanosecond is shown in Figure 2 for negative point corona.

B. Corona from the end of a cylindrical conductor

1. Description of experiments

Experiments were performed on 10 and 20 foot lengths of 2-1/4 inch diameter aluminum pipe with the following objectives:

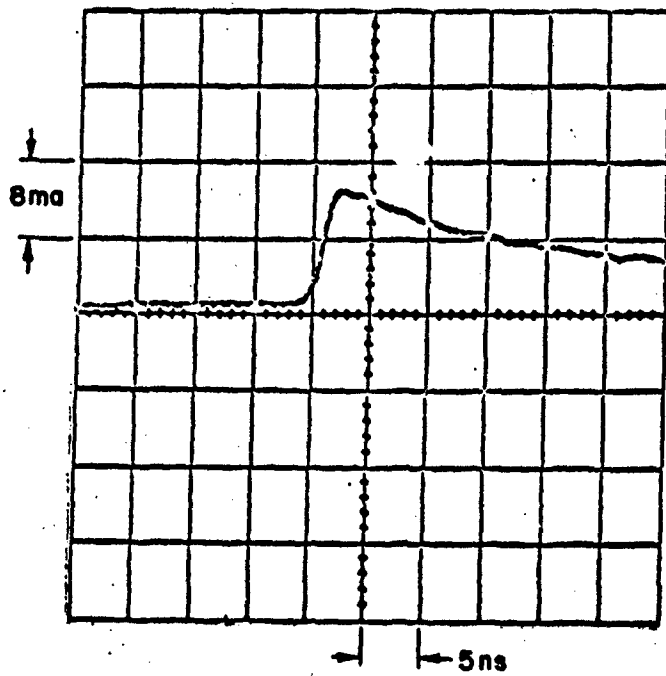
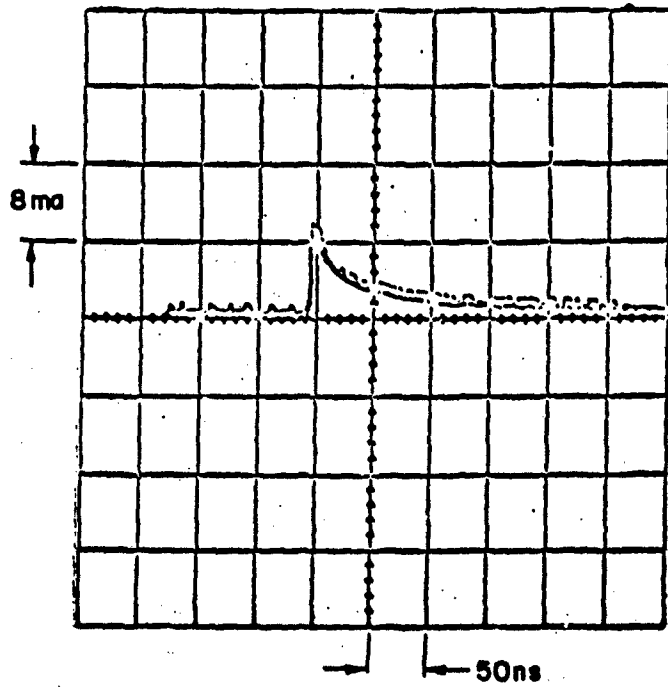
- a. Verify the pulsed transmission line model of the current distribution.
- b. Measure the corona repetition rate and d.c. charging current as a function of the charging voltage.
- c. Measure the radiated power in the far zone ($d > 1.2 \times$ wavelength) of the cylinder.

The work was done at the Cherry Creek Field Site with the pipe supported horizontally or vertically by an insulated stand. One end of the pipe was capped with a spherical conductor and the other was tapered to a point. Voltages of up to -50 KV were applied through a charging coil so that any transient current pulses initiated by a corona discharge at one end would travel on the pipe rather than through the power supply.

2. Current distribution

The current distribution on the pipe was measured by mounting the 20 foot pipe horizontally 1 meter above a wire mesh ground screen and recording the radial electric field at the ground directly below the pipe. For this geometry the radial electric field and current are related by the equation⁽¹⁾

$$e(t) = \frac{120 i(t)}{h}$$



6
FIGURE 2 NEGATIVE POINT CORONA CURRENT PULSE

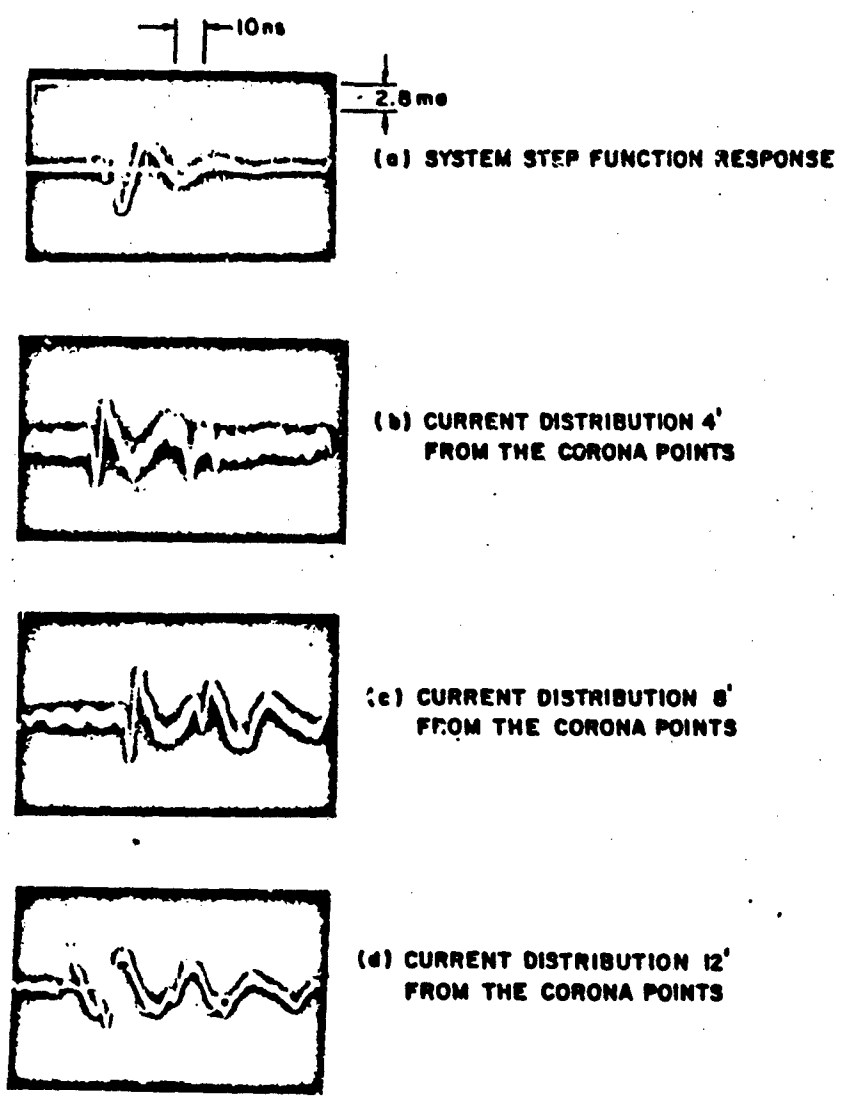
where h is the distance to the ground plane.

The E-field measurements were made with a short probe antenna which fed a high impedance preamplifier, followed by a 40 MHz high pass filter to reduce the background noise from commercial radio transmissions. The output was recorded on film with a Tektronix 454 oscilloscope. The overall system passband was 40 to 150 MHz for this experiment.

Measurements were obtained with the probe at distances of 4, 8, and 12 feet from the corona point. The results are shown in Figure 3, along with the system response to a step function of voltage. The initial pulse and reflections from the open ends of the pipe are seen to occur as expected. The reflection time delays correspond to the pulse travel time from the observation point to the ends of the pipe and back at approximately the speed of light. The system sensitivity was such that a field strength of 3.3 volts/meter corresponded to 1 volt deflection on the oscilloscope. The 170 mv amplitude of the first pulse corresponds to a current pulse of 5 milliamps. The first reflection from the end of the pipe arrived before the initial pulse had died out completely. This distorted the amplitude of the reflected pulse; however the distortion is low at the 4 foot position where the time separation is maximum. The ratio of the reflected to initial pulse amplitude at this point gives a reflection coefficient of approximately 0.8. The reflection coefficient would be unity in the ideal case.

3. Corona pulse rate and charging current

The corona pulse rate and d.c. charging current on the 20 foot pipe were measured at pipe voltages between -6 KV and -30 KV. Trigger pulses were picked up from a small metal plate placed approximately 10 cm from the corona point and grounded through a 50 ohm resistor. The voltage pulse across the resistor caused by induced current in the plate was amplified and used to trigger an electronic counter.



7
FIGURE 3 CURRENT DISTRIBUTION ON 20' PIPE



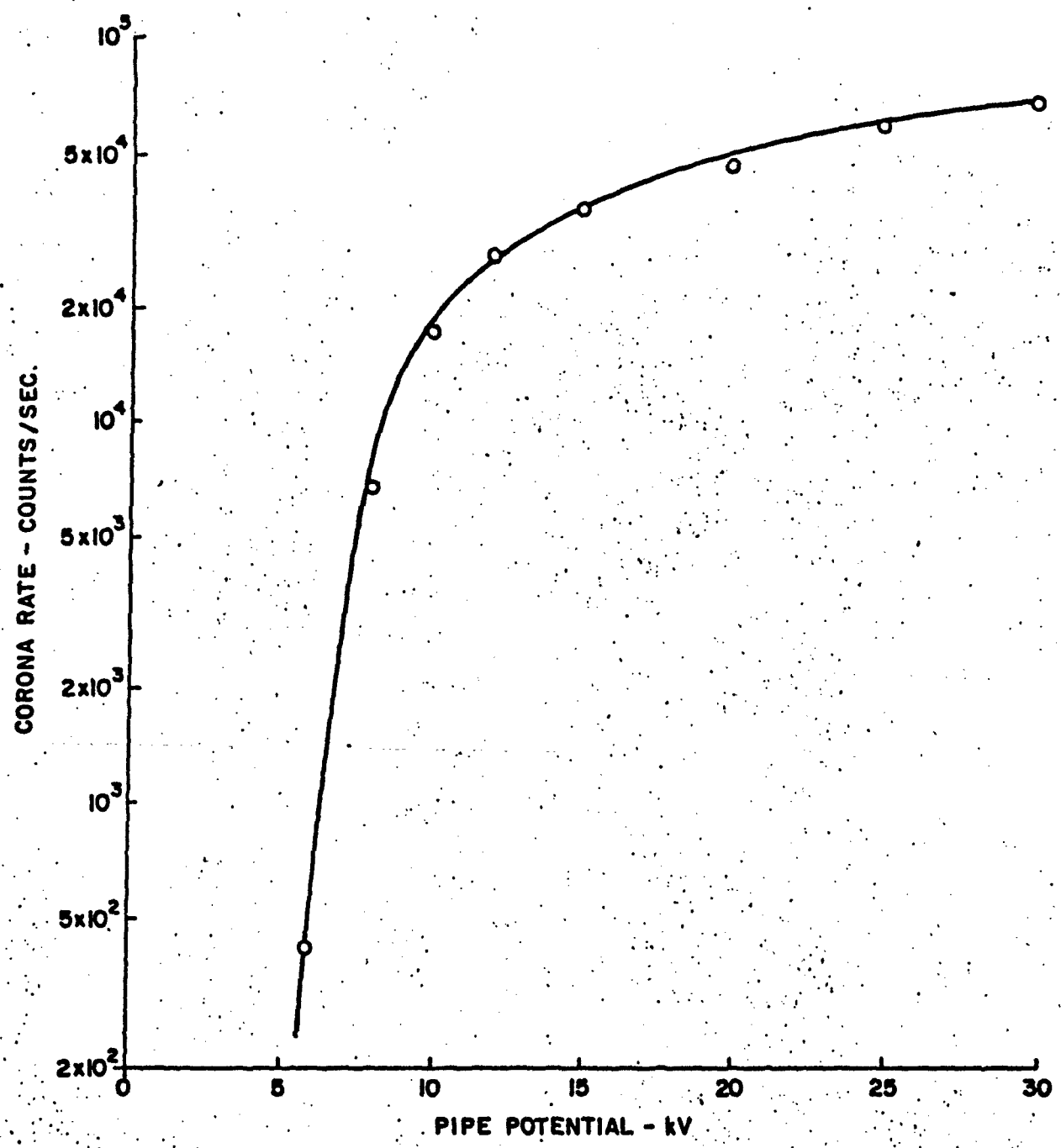
The average pulse rate as a function of the charging voltage is shown in Figure 4. The rate increases sharply once the corona threshold voltage of approximately -5 KV is exceeded.

The charging current and average current per pulse as a function of voltage are shown in Figure 5. The increase in the average current per pulse as the voltage increases is consistent with an expected increase in the number of electron avalanches per pulse as the field energy increases.

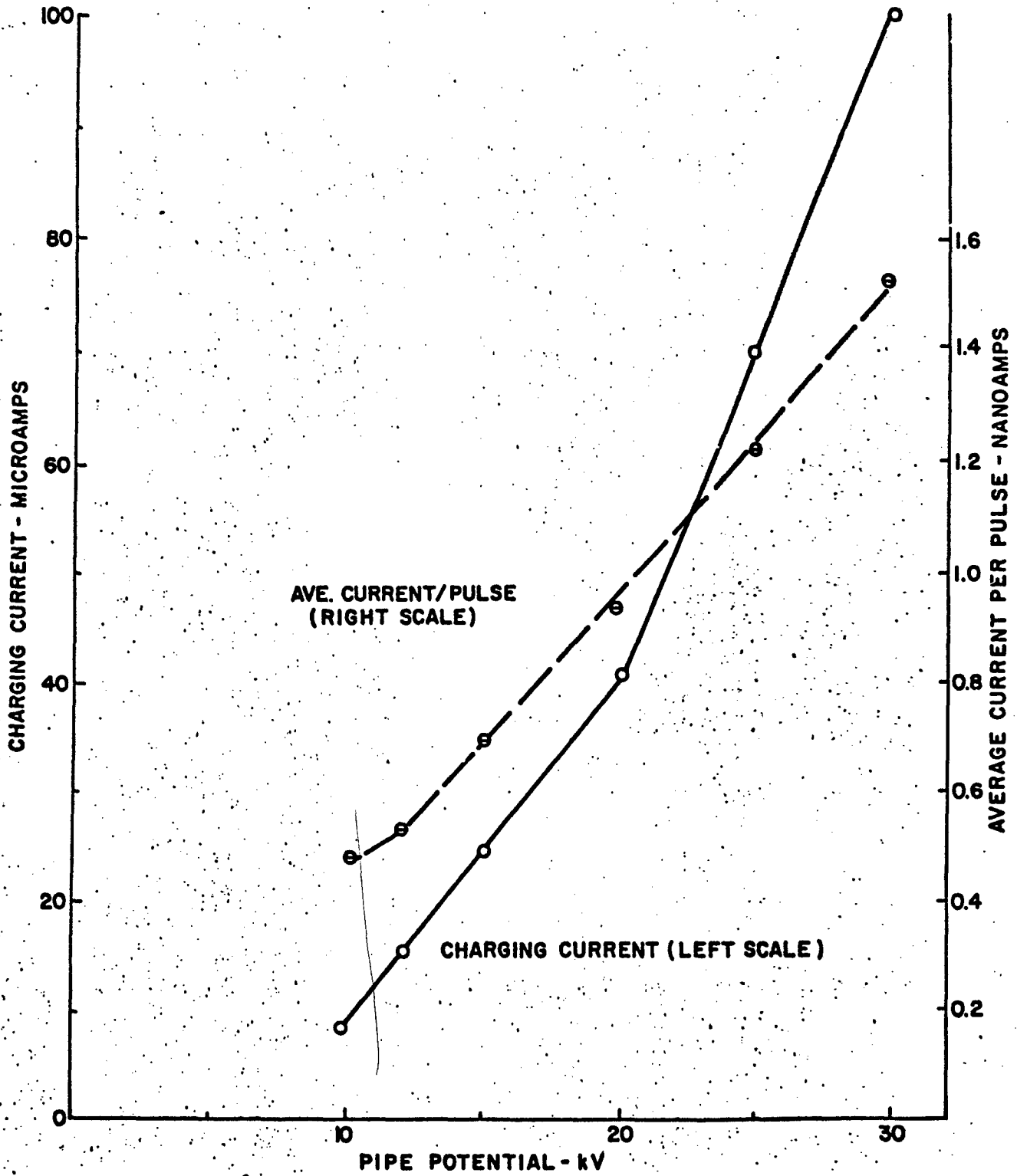
4. r-f radiation

The power radiated by vertical 10 foot and 20 foot lengths of pipe was measured at distances of 25 and 50 feet. At these distances the far field is a factor of 10 greater than the near field at frequencies above 47 MHz at 25 feet and 24 MHz at 50 feet. The measurements were made with a log-periodic antenna with a gain of 12 db, designed for the 30 to 300 MHz frequency range. The instrumentation consisted of a low noise preamplifier, 150 feet of RG-8 coax cable, and an HP8555A spectrum analyzer. The data were recorded by photographing the display scope of the spectrum analyzer when it was operated in a swept-frequency mode, or by photographing the detected I.F. output on an auxiliary scope when it was operated as a fixed tuned receiver. The system, excluding the antenna, was calibrated with a VHF signal generator over the 10 to 480 MHz frequency range.

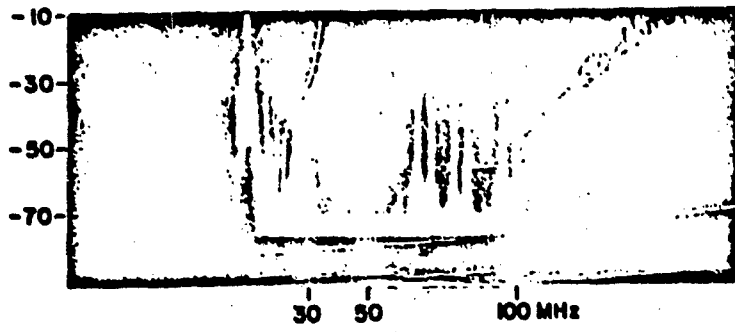
Swept frequency recordings of the power received in a 300 kHz pass band from the 10 foot pipe are shown in Figure 6. The upper trace (a) shows the normal background noise level at the Cherry Creek Field Site with a fairly quiet zone between approximately 25 and 60 MHz. Trace (b) was recorded at 25 foot with a single corona point at the upper end of the pipe. The lower spherically capped end was 24" above ground level. Traces (c)



8
FIGURE 4. CORONA PULSE RATE VERSUS PIPE POTENTIAL



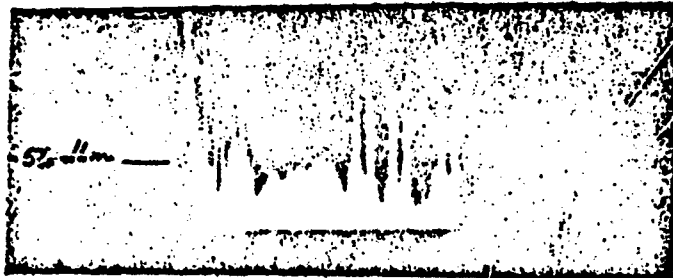
9
FIGURE 5. CHARGING CURRENT VERSUS PIPE POTENTIAL



(a) BACKGROUND NOISE (dbm)



(b) CORONA NOISE AT 25'
SINGLE POINT AT TOP



(c) CORONA NOISE AT 25'
SINGLE POINT AT BOTTOM



(d) CORONA NOISE AT 50'
SINGLE POINT AT BOTTOM

¹⁰
FIGURE 6 R-F POWER RECEIVED FROM A 10' PIPE IN CORONA

and (d) show the noise power at 25 feet and 50 feet respectively with the corona point at the lower end of the pipe.

The pipe potential was held at -25 KV for these experiments. A broad spectrum of corona noise is seen at levels of 15 to 20 db above the background level over the 25 to 60 MHz frequency range where the background is low (-75 dbm). The reduction in peak amplitude of approximately 6 db between the 25 foot and 50 foot recording distances is consistent with the expected 6 db change that should occur in the radiation zone when the distance is doubled. No significant differences are observed between traces (b) and (c) which correspond to corona from the top and the bottom of the pipe.

The power measurements obtained with the spectrum analyzer are related to the incident field by the equation

$$E_i = \frac{5.7 \times 10^{-13} f_o \sqrt{P}}{g} \quad 2-2$$

where E_i = spectral amplitude of the incident field (v-sec/m),

f_o = receiver center frequency (Hz),

P = recorded power (Watts),

g = voltage gain of the receiving system.

Equation (2-2) is based on the assumption that the spectral amplitude E_i is constant over the receiver pass band and that the antenna gain was 12 db. As an example, a recorded power level of -60 dbm at a frequency of 50 MHz corresponds to an incident field of 3×10^{-10} v-sec/m*.

Strong interference at frequencies above 60 MHz prevented measurement of the corona spectrum at higher frequencies using the swept frequency mode. However, with the receiver tuned manually to frequency

* The system gain at 50 MHz was a factor of 3.

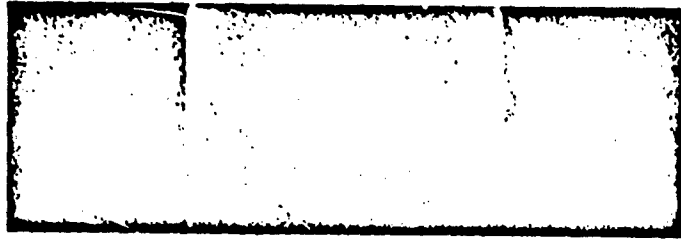
points where the interference was relatively low, the corona noise could be detected by observing the detected I.F. output of the spectrum analyzer. With this technique, corona noise could be observed at frequencies up to approximately 120 MHz. Examples of the detected output in a 300 kHz pass band are shown in Figure 7 for center frequencies of 30, 50, 75, and 100 MHz. These data were recorded at a distance of 25 feet from the 20 foot pipe, which was held at a potential of -8 KV.

The data presented here were all recorded with the radiating structure and receiving antenna oriented vertically over soil of average conductivity. The fields are therefore approximately doubled over those that would be observed from the same structure in the absence of the ground. Some attempts were made to record the corona noise with the antennas parallel to the ground; however, the ground reflected signal in this case nearly cancels the direct signal after a time delay which is proportional to the ray path difference between the direct and ground reflected field components. The time delays for the source-receiver geometries that could be practically attained was just a few nanoseconds and no data were recorded from the horizontal configuration. This problem is discussed in more detail in Section III of this report.

C. Radio Noise Survey

1. Description of experiments

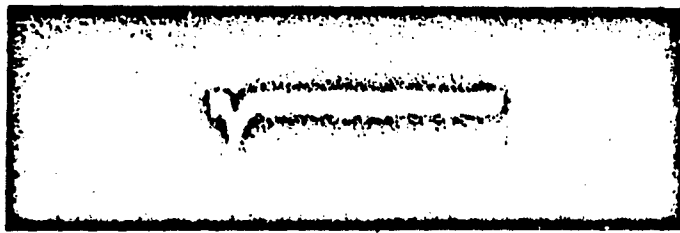
Experiments designed to measure the natural noise background in the 30 to 350 MHz frequency range were carried out aboard the R/V Acania, a research vessel operated by the Department of Oceanography of the Naval Postgraduate School, Monterey, California. The primary goal was to record the broadband impulsive background noise at sea with a secondary objective of measuring background noise at narrower bandwidths on a swept frequency basis.



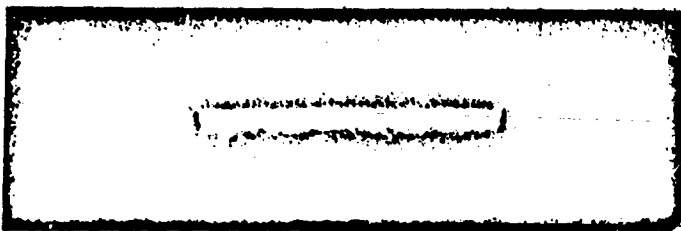
(a) 30 MHz CENTER FREQUENCY
0.1 mv/div
5 μ s/div



(b) 50 MHz CENTER FREQUENCY
0.1 mv/div
5 μ s/div



(c) 75 MHz CENTER FREQUENCY
0.05 mv/div
5 μ s/div



(d) 100 MHz CENTER FREQUENCY
0.05 mv/div
5 μ s/div

11
FIGURE 7. DETECTED I.F. SIGNALS RECEIVED FROM A 20' PIPE IN CORONA

The broadband measurement system consisted of a short vertical monopole antenna which fed a high impedance preamplifier, pulse amplifiers, and a Tektronix 485 oscilloscope. The system pass band was 30 MHz to 450 MHz. The narrow band swept frequency system utilized a log-periodic antenna and a HP8555A spectrum analyzer which covered the 50 to 500 MHz frequency range.

2. Results

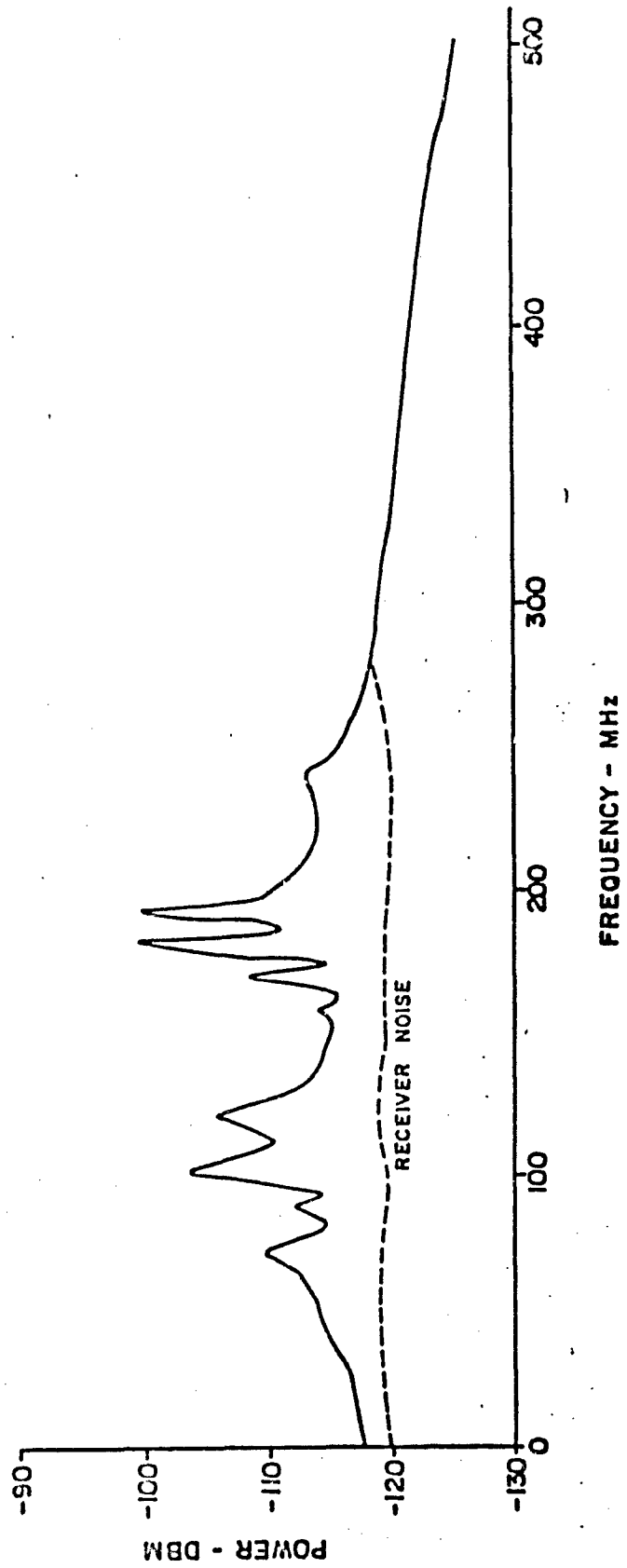
The experiments were performed in July 1975 at a maximum distance from shore of 120 miles. Figure 8 shows a typical swept frequency plot of the noise received in a 300 kHz pass band using the narrow band system. Man-made noise at levels of -100 to -120 dbm predominated at this distance from shore over much of the frequency range studied. At closer distances the noise was higher and consisted solely of man made signals.

Measurements of the impulsive background noise were unsuccessful because of the limited distance from shore of the Acania. Television and/or FM broadcast station signals at the maximum distance of 120 miles were still much stronger than the impulsive background noise at this distance.

D. Field Measurements on Low Flying Aircraft

1. Description of Experiments

The measurement of noise generated by aircraft in flight was attempted with available instrumentation after modifying the HP8555A spectrum analyzer to give a 10 MHz I.F. bandwidth. The recording system, using the log-periodic antenna, was set up at a distance of 100 meters South of the East end of the East-West runway at Stapleton International Airport in Denver. Observations were made on several occasions during varied weather conditions. The analyzer was tuned to relatively quiet frequency spots near 150 MHz or 275 MHz and the i.f. output was monitored on an oscilloscope.



12-
 FIGURE 8. BACKGROUND NOISE SPECTRUM MEASURED AT SEA

Approved for Release by NSA on 05-08-2014 pursuant to E.O. 13526

2. Results

Signals consisting of bursts of random appearing pulses, often accompanied by a short quasi-CW burst were observed on several occasions as aircraft flew through the antenna beam. The most consistent observations were obtained during a two hour period when light rain was falling. Nearly all of the aircraft gave detectable signals during this period, whereas only the larger aircraft such as DC-10's or 747's were detectable during balmy weather. It was observed that automobile ignition noise was generally detectable at considerably greater distances than were aircraft.

Although these experiments involved a large number of variables which could not be controlled, strong correlation was observed between the passage of an aircraft through the antenna beam and the noise output of the recording system. However, the recorded noise could not be definitely attributed to corona as no independent method was available to determine whether or not the aircraft were actually in corona at the time the observations were made.

III. ANALYSIS

A. The corona current in air

A corona discharge from a negatively charged conductor produces electronic and ionic currents in the air near the corona point by electron avalanching. The current is dominated initially by the motion of the electrons and latter by the build up of heavy positive and negative ions. Photons emitted by the corona envelope cause further ionization of the air and also release new electrons from the conductor by photoemission. The net result is a very fast rising pulse of current during the electronic phase which decays exponentially in time during the ionic phase of the discharge. Only the electronic current component has been studied here, since it is much faster and contributes most of the high frequency content of the radiated pulse.

The electron current density in air was calculated by solving Townsends equations for an electron in a non-uniform electric field between a negatively charged point and a grounded plane. ⁽²⁾

The result is given by the equation

$$J(x', t') = qn_0 \delta(t' - \tau) \exp \left\{ (Ap/C_1) \left[1 - \exp(-C_1 X') \right] \exp(-C_1 a) \right\} \quad 3.1$$

where

q = electron charge (1.602×10^{-19} coulombs)

n_0 = number density of initial electrons (electrons/cm²)

A = constant (14.6)

p = atmospheric pressure (760 mm)

C_1 = constant (160)

a = radius of corona point (0.01 cm)

The parameter τ was determined from the differential equation for the electron velocity and from the mobility equation, which relates the velocity to the electric field. The solution gives

$$\tau = \frac{C_1(2ax' + x'^2)}{2Bpb} \quad 3.2$$

where

b = electron mobility (500 cm/sec per volt/cm),

B = constant (365).

B. The corona current on a conducting cylinder

The pulse of current launched onto a conductor when a corona discharge occurs can be determined by equating the work done by the field to the change in energy of the charged conductor. This gives

$$I(t') = \frac{1}{V} \int E(x') J_1(x', t') d^3x' \quad 3.3$$

where $I(t')$ is the current pulse on the conductor. This equation was evaluated by substituting equation 3.1 for J_1 and approximating the field distribution by the equation

$$E(x') = \frac{V}{(a+x') \ln(2l/a)} \quad 3.4$$

which is a sufficient approximation for the field between a point of radius "a" raised to a potential V and a plane at a distance l from the point. (3)

With these substitutions the integral in equation 3.3 evaluates to

$$I(t') = \frac{I_0 \exp \left\{ (Ap/C_1) \left[1 - \exp(-C_1 \sqrt{a^2 + 2BpbI'/C_1} - a) \exp(-C_1 a) \right] \right\}}{a^2 + 2BpbI'/C_1} \quad 3.5$$

where

$$I_0 = \frac{\pi d^2 q n_0 Bpb}{C_1 \ln(2l/a)} \quad 3.6$$

The corona channel was assumed to be cylindrical of radius d (cm) in this derivation. The current pulse given by equation 3.5 is shown plotted in

Figure 9, using appropriate values for the various constants in equations 3.5 and 3.6, consistent with a typical discharge. ⁽⁴⁾

C. The radiated fields

The fields radiated by the corona current in air, and the current on the cylinder have been calculated separately by evaluating the vector potential for each case. The vector potential is given by the equation ⁽⁵⁾

$$A_{1,2}(r,t) = \frac{1}{c} \int d^3x' \int dt' \left\{ \frac{J_{1,2}(x',t') \delta(t' + r/c - t)}{r} \right\} \quad 3.7$$

where the subscript 1 applies to the corona current in air and the subscript 2 applies to the current on the cylinder. The constant c is the speed of light and the primed and unprimed variables refer to the source and receiver coordinates respectively. The distance r is measured from the current element $J(x',t')$ to the receiving point. The geometry is shown in Figure 10.

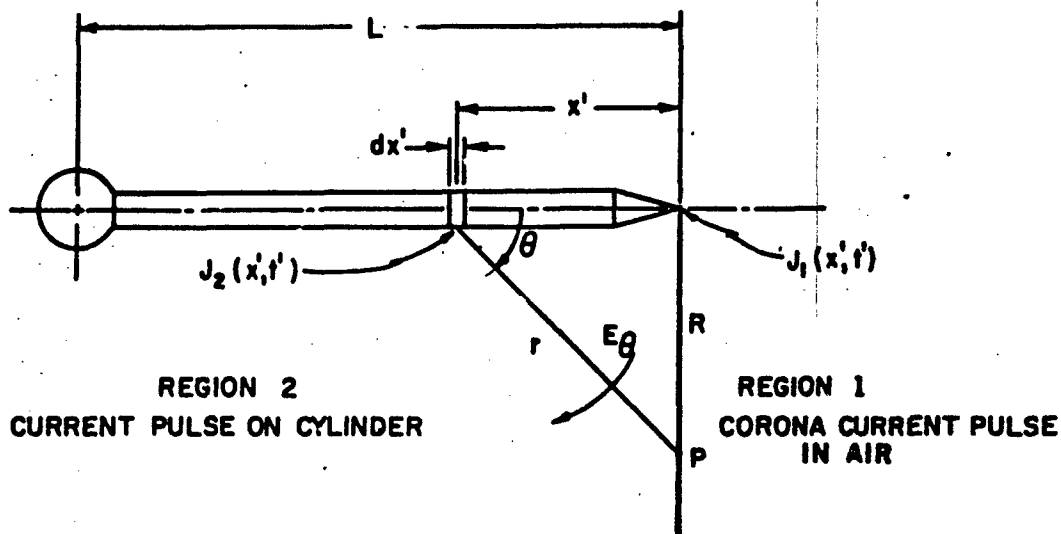


Figure 10. Source Geometry

The electric field component E_θ in the radiation zone is related to the vector potential by the equation

$$E_\theta = -\frac{1}{c} \frac{\partial A}{\partial t} \quad 3.8$$

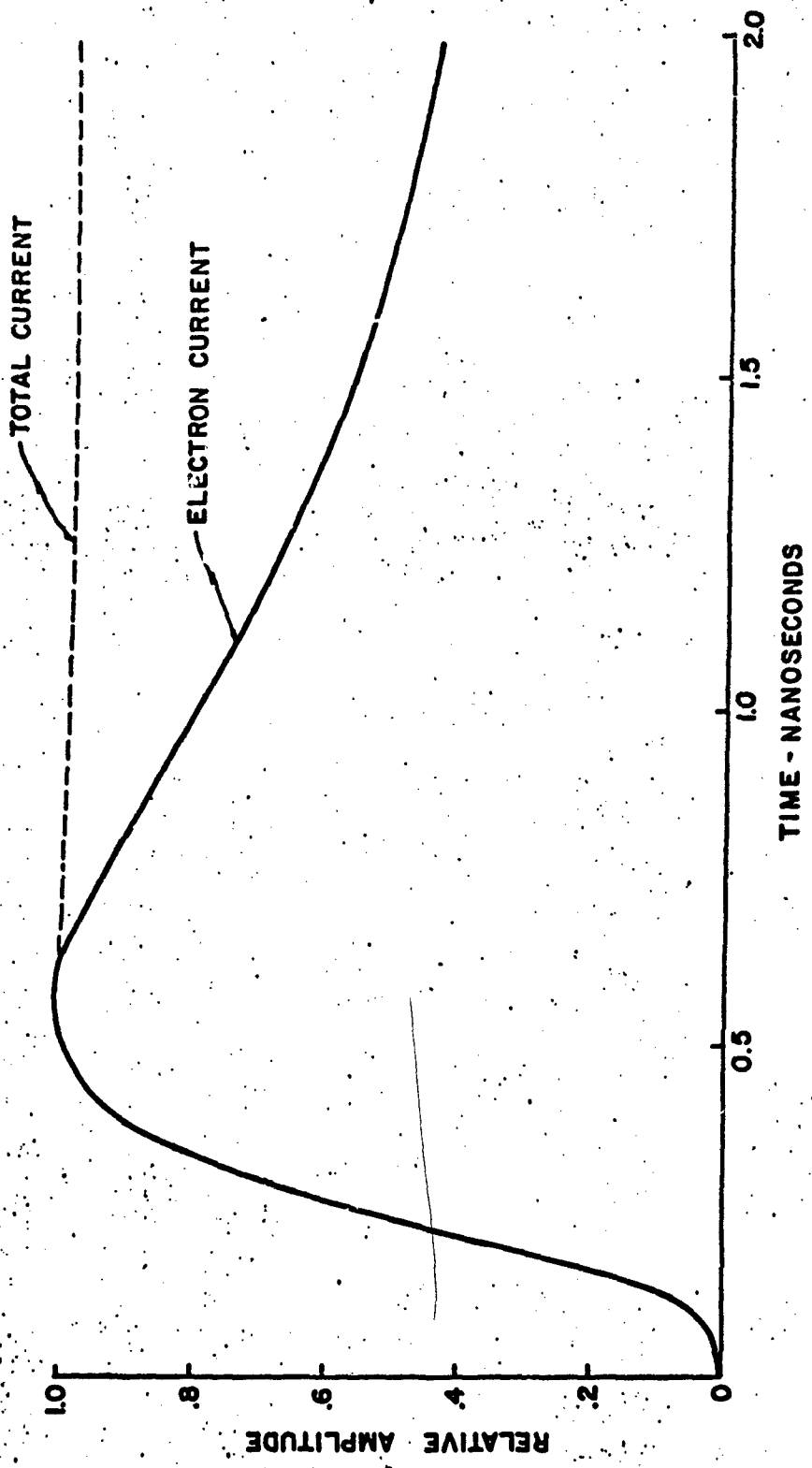


FIGURE 9. CALCULATED CURRENT PULSE ON A CYLINDER



and the magnetic field H_ϕ is then given by $H_\phi = E_\theta / (120\pi)$. 3.9

The integration of equation 3.7 was carried out directly in the time domain in region 1, using equation 3.1 for J_1 . The final result can be written in the form

$$e_1(t) = \frac{m C_3 \exp \left\{ C_2 \exp (-C_1 \sqrt{a^2 + mt}) \right\}}{2 c^2 R (a^2 + mt)} \quad 3.10$$

$$\left\{ C_1 C_2 \exp (-C_1 \sqrt{a^2 + mt}) + \frac{1}{\sqrt{a^2 + mt}} \right\} \sin \theta$$

where $m = 2 B p b / C_1$ 3.11

$$C_2 = -A p / C_1 \quad 3.12$$

$$C_3 = n_0 \pi d^2 q m \exp \left[-C_2 \exp (-C_1 a) \right] / 2 \quad 3.13$$

and the approximations

$$r \approx R (1 - x' \cos \theta / R) \quad 3.14$$

$$d^3 x' \approx \pi d^2 dx' \quad 3.15$$

$$x/R \ll 1 \quad 3.16$$

have been used. Equation 3.10, which gives the electric field pulse radiated by the corona current in air is shown plotted in Figure 11.

The fields radiated by the current on the cylinder in region 2 were computed in the frequency domain and then transformed back into the time domain. For this case the vector potential has the form

$$A(R, \omega) = \frac{K(\omega) \exp(-kR) \int dx' I(x') \exp(-kx' \cos \theta)}{CR} \quad 3.17$$

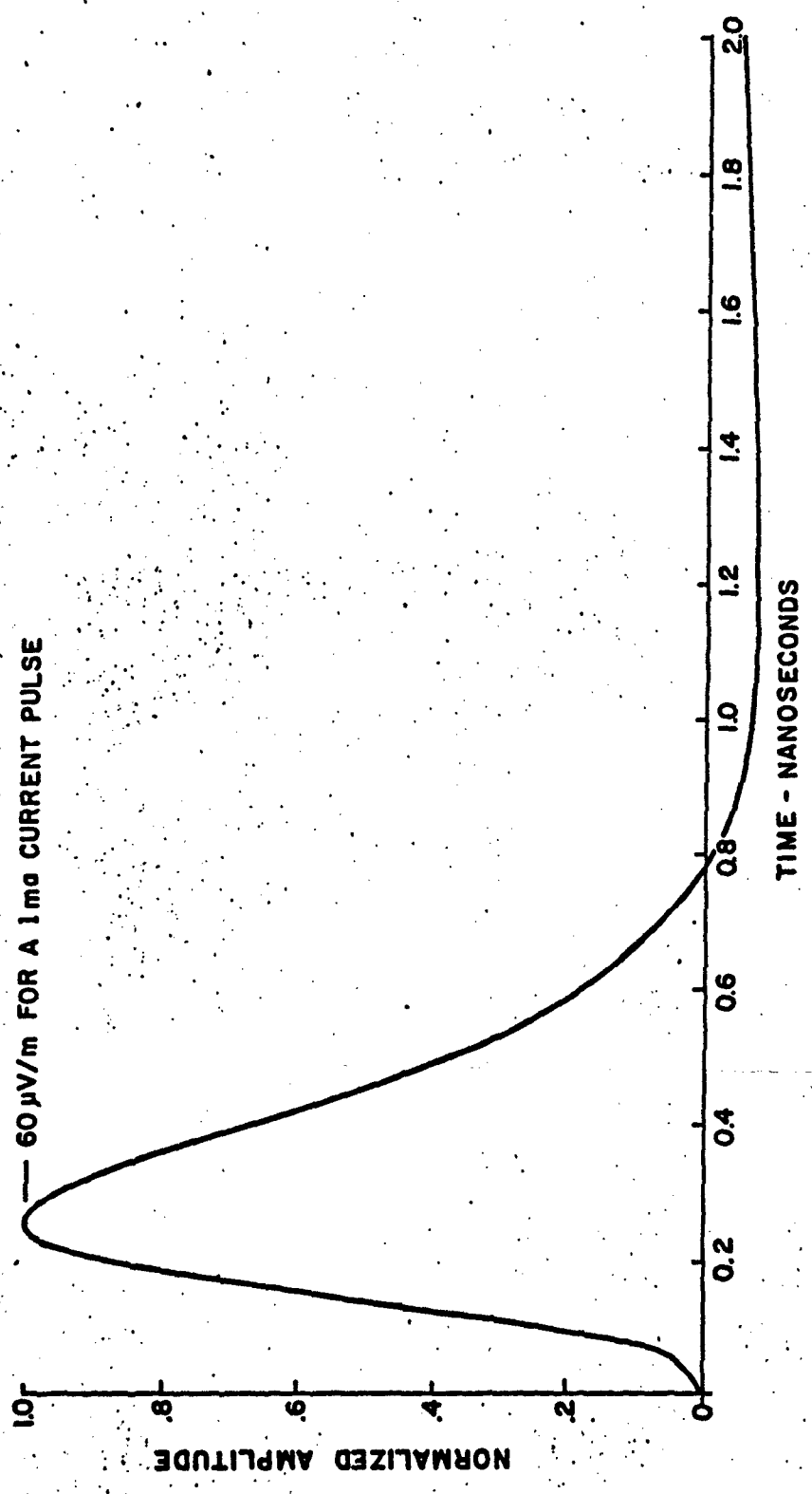


FIGURE 11. RADIATED PULSE FROM CORONA ELECTRON CURRENT IN AIR

where $K(\omega)$ is the spectrum of the current pulse defined by equation 3.5 and plotted in the time domain in Figure 9.

$I(x')$ is the current distribution along the cylinder and $k = \omega/c$ is the propagation constant in free space. $I(x')$ can be determined from transmission line theory, which for a thin cylinder has the form⁽⁶⁾

$$\begin{aligned} I(x') = & \exp(-\gamma x') + T_1 \exp[-\gamma(2L-x')] + T_0 T_1 \exp[-\gamma(2L+x')] \quad 3.18 \\ & + T_0 T_1^2 \exp[-\gamma(4L-x')] + T_0^2 T_1^2 \exp[-\gamma(4L+x')] \\ & + T_0^2 T_1^3 \exp[-\gamma(6L-x')] + \dots \end{aligned}$$

The substitution of equation 3.18 into 3.17 and evaluation of the integral gives the vector potential in region 2. The radiated electric field at point P is then determined from equation 3.8. The result is

$$\begin{aligned} E(R, \omega) = & \frac{L \sin \theta}{2Rc^2} \exp(-ikR) (i\omega) K(\omega) \left\{ \frac{\sin kz_1}{kz_1} \left[\exp(-ikz_1) \right. \right. \\ & \left. \left. + T_0 T_1 \exp(-ik(2L+z_1)) + \dots \right] \right. \quad 3.19 \\ & \left. + \frac{\sin kz_2}{kz_2} \left[T_1 \exp(ik(2L-z_2)) + T_0 T_1^2 \exp(-ik(4L-z_2)) + \dots \right] \right\} \end{aligned}$$

The above results pertain to a cylinder of length L where T_0 is the reflection coefficient at the corona end of the cylinder and T_1 is the reflection coefficient at the opposite (open) end. γ is the transmission constant given by

$$\gamma = \alpha + ik \quad 3.20$$

where α gives the attenuation and k is the phase constant of the cylinder when treated as a transmission line. The variables Z_1 and Z_2 are defined by the equation

$$Z_{1,2} = L(1 \pm \cos \theta)/2 \quad 3.21$$

For the special case $\theta = \pi/2$, $Z_1 = Z_2 = L/2$ and equation 3.19 can be written in MKS units as

$$E(R, \omega) = \frac{30K(\omega)}{R} (\sin \pi L/\lambda) \left\{ \exp[-ik(R+L/2)] + \dots \right\} \quad 3.22$$

where the terms in braces correspond to the successive reflections from the two open ends of the cylinder.

The inverse transform of equation 3.19 gives the time domain solution. This is most easily obtained by using the time convolution theorem for the products of frequency functions, which has the notation

$$f_1(t) * f_2(t) * \dots \longrightarrow F_1(\omega) \cdot F_2(\omega) \cdot \dots \quad 3.23$$

where the asterisk denotes convolution and the arrow signifies the Fourier transform. The final result in MKS units can be written

$$e(R, t) = \frac{15}{R} i(t) * \left\{ \frac{\sin \theta}{1 + \cos \theta} \left[\delta(t^*) - \delta(t^* - 2Z_1/C) + T_0 T_1 \delta(t^* - 2L/C) \right. \right. \\ \left. \left. - T_0 T_1 \delta(t^* - 2L/C - 2Z_1/C) + \dots \right] \right. \\ \left. + \frac{\sin \theta}{1 - \cos \theta} \left[T_1 \delta(t^* - 2L/C + 2Z_2/C) - T_1 \delta(t^* - 2L/C) + \dots \right] \right\} \quad 3.24$$

where $t^* = t - R/C$.

The reflection coefficients T_0 and T_1 have been assumed independent of frequency in equation 3.24, so that only the amplitude and not the shape of the current pulse $i(t)$ is changed upon reflection.

The form of equation 3.24 is convenient for computations because the convolution of the current pulse $i(t)$ with the string of delta functions contained within the braces simply superimposes the pulses, each shifted in time to that given by the argument of each delta function. The results for the special case $\theta = \pi/2$ and $T_0 = T_1 = -0.8$ are depicted diagrammatically in Figure 12.

All of the calculations have been carried out for a conductor in free (air) space. The results for a conductor near the earth would be modified by the image currents in the ground. The effect on the radiated signal from a vertical conductor over ground of finite conductivity would be to increase the signal amplitude by the factor $(1+R)$, where R is the ground reflection coefficient, which is positive for vertical polarization. For infinite conductivity, $R = +1$ and the signal amplitude would be doubled.

The horizontally polarized field radiated by an elevated conductor mounted parallel to the earth's surface can also be estimated. For this case the ground reflection coefficient is approximately equal to -1 for all frequencies. The resultant field at an elevated receiving antenna, which is the sum of a direct and a ground reflected component, would be proportional to the derivative of the free space field over a restricted frequency range. This can be seen from the equation

$$E(t) = e(t) + Re(t-\tau) \quad 3.25$$

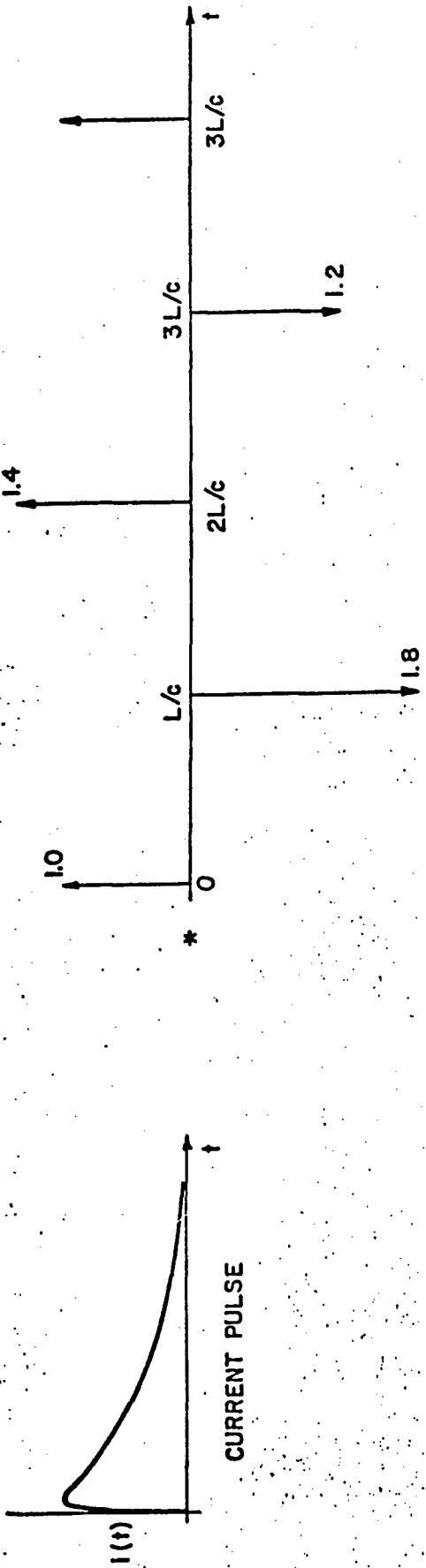
where

$e(t)$ is the free space field,

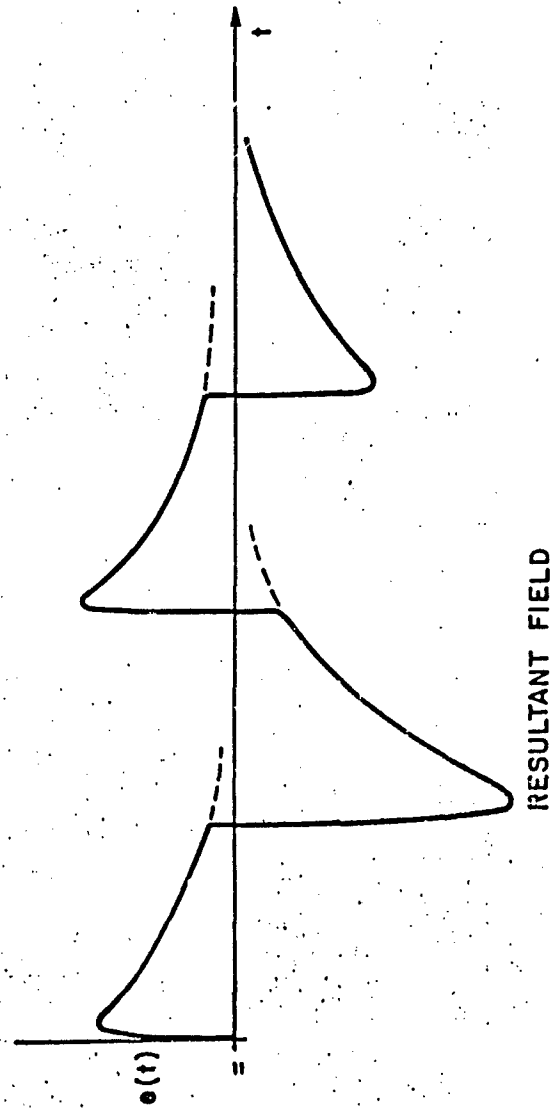
R is the reflection coefficient for horizontal polarization ($R = -1$),

τ is the path difference delay time.

$E(t)$ is the resultant field at the antenna.



DISTRIBUTION FUNCTION



RESULTANT FIELD

FIGURE 12. SYNTHESIS OF THE RADIATED PULSE TRAIN BY CONVOLUTION



The substitution $t' = t + \tau/2$ and $R = -1$ gives

$$E(t') = e(t' + \tau/2) - e(t' - \tau/2) \quad 3.26$$

which has the Fourier transform

$$G(\omega) = i\omega\tau F(\omega) \frac{\sin(\omega\tau/2)}{\omega\tau/2} \quad 3.27$$

where $G(\omega)$ is the Fourier transform of $E(t)$ and $F(\omega)$ is the Fourier transform of $e(t)$. When $\omega\tau$ is small,

$$G(\omega) \approx i\omega\tau F(\omega) \quad 3.28$$

which transforms back into the time domain as

$$E(t) \approx \tau \frac{de(t)}{dt} \quad 3.29$$

This shows that the resultant horizontal field at the antenna is approximately proportional to the derivative of the free space field. The frequency range over which 3.27 is valid is determined by the sinc function. Thus for 10% accuracy the requirement is

$$0.9 \leq \text{sinc}(\omega\tau/2) \leq 1 \quad 3.30$$

which is met when $f\tau \leq 0.25$. As an example, if the time difference τ was 5 nanoseconds, the resultant field would be proportional to the derivative (within 10%) for frequencies

$$f \leq 0.25/(5 \times 10^{-9}),$$

or

$$f \leq 50 \text{ MHz.}$$

An order of magnitude estimate of the radiated spectral amplitude $E(R, \omega)$ can be obtained from equation 3.22 once the spectrum $K(\omega)$ of the current pulse is known. This could be computed numerically from the recorded corona current pulse shown in Figure 2; however, for the frequency range of

interest, the pulse is adequately represented in closed form by the double exponential function

$$i(t) = i_0 [\exp(-at) - \exp(-bt)] \quad 3.31$$

which has the Fourier transform

$$K(\omega) = \frac{i_0}{a - \omega^2/b - i\omega} \quad 3.32$$

where i_0 is the peak amplitude of the current pulse and the decay constants a and b have the values

$$a = 3.3 \times 10^7, \quad b = 9.4 \times 10^9. \quad \text{With } i_0 = 5 \text{ ma, } f = 50 \text{ MHz,}$$

the magnitude of the spectrum is

$$|K(f)| = 1.6 \times 10^{-11} \text{ amp-sec} \quad 3.33$$

Substitution of this value into equation 3.22 gives

$E(f) = 2 \times 10^{-9}$ v-sec/m at 1 meter for a single pulse train radiated by a cylinder of length $L = 10$ feet.

IV. CONCLUDING REMARKS

The radiation from a conducting cylinder in corona at one end has been measured and found to be in good agreement with calculations of the current pulse which travels on the cylinder and the transmission line model of the current distribution. As an example, the -56 dbm power level measured at 50 MHz, with the receiving antenna at a distance of 25 feet from the 10 foot pipe corresponds to a spectral amplitude of 3.6×10^{-9} v-sec/m at 1 meter. This compares very well with the calculated value of approximately 4×10^{-9} v-sec/m for a vertical cylinder over a perfect ground plane. For a random discharge rate of 100 kHz, the incident flux density would be approximately 4×10^{-15} watts-sec/m² compared to a background noise flux from atmospheric and galactic noise of approximately 1.4×10^{-19} watts-sec/m² in the 50 to 100 MHz frequency range. (7)

Cylinders were used in these experiments because the simple geometry involved is amenable to calculation. More complicated structures such as airframes would be expected to behave differently; however, the basic transmission line model is directly applicable to more complicated geometrical shapes. Scaled models of aircraft could be used to determine many of the characteristics of the radiated fields expected from full scale aircraft in corona.

The charging current and potential of the cylinders studied were much lower than the nominal values given for aircraft in flight. (8) It is reasonable to expect that the incident noise flux from an airplane in corona would be considerably more intense than the flux which has been determined from these experiments with cylinders.

REFERENCES

1. Scheikunoff, S.A. and Friis, H.T., "Antennas, Theory and Practice," Wiley and Sons, New York, 1952.
2. Raether, H., "Electron Avalanches and Breakdown in Gases," Butterworth and Company, London, 1964.
3. Tamura, T., Proc. Phys. Soc. (Japan), 16, 2503 (1961).
4. Loeb, L.B., "Electrical Coronas, Their Basic Physical Mechanisms," Univ. of Cal. Press, 1965.
5. Jackson, J.D., "Classical Electrodynamics," Wiley and Sons, New York, 1962.
6. Page, L. and Adams, N.I., "Principles of Electricity," D. Van Nostrand Co., New York, 1949.
7. Findley, J.W., "Antennas and Receivers for Radio Astronomy," in "Advances in Radio Research," Vol. 2, (J.A. Saxton, ed.), Academic Press, New York, 1964.
8. Tanner, R.L., and Nanevicz, J.E., Proc. IEEF, 52, 44 (1964).

END

FILMED

1-85

DTIC